Experiments and modeling of by-pass pigging under low-pressure conditions

Hendrix, M. H.W.; IJsseldijk, H. P.; Breugem, W. P.; Henkes, R. A.W.M.

DOI
10.1016/j.jprocont.2018.08.010

Publication date
2018

Document Version
Final published version

Published in
Journal of Process Control

Journal of Process Control 71 (2018) 1–13

Contents lists available at ScienceDirect

Journal of Process Control

journal homepage: www.elsevier.com/locate/jprocont

Experiments and modeling of by-pass pigging under low-pressure conditions

M.H.W. Hendrix [a,*], H.P. IJsseldijk [a], W.-P. Breugem [a], R.A.W.M. Henkes [a,b]

[a] Laboratory for Aero and Hydrodynamics, Delft University of Technology, Leeghwaterstraat 21, 2628 CA Delft, The Netherlands
[b] Shell Technology Centre Amsterdam, Amsterdam, The Netherlands

ARTICLE INFO

Article history:
Received 6 January 2018
Received in revised form 23 July 2018
Accepted 28 August 2018
Available online 22 September 2018

Keywords:
Low pressure
By-pass pig
Pipeline maintenance

ABSTRACT

We present experimental and numerical results for by-pass pigging under low-pressure conditions which aided the design of a speed-controlled pig (Pipeline Inspection Gauge). Our study was carried out using air as working fluid at atmospheric pressure in a 52 mm diameter pipe of 62 m length. The experimental results have been used to validate simplified 1D models commonly used in the oil and gas industry to model transient pig behaviour. Due to the low pressure conditions oscillatory behavior is observed in the pig speed, which results in high pig velocity excursions. The oscillatory motion is described with a simplified model which is used to design a simple controller aimed at minimizing these oscillations. The controller relies on dynamically adjusting the by-pass area, which allows to release part of the excess pressure which builds up in the gas pocket upstream of the pig when the motion of the pig is arrested. Subsequently, the control algorithm is tested by a 1D transient numerical model and it was shown to successfully reduce the pig velocity excursions.

1. Introduction

Pipelines are used in many industries as a means of transporting fluids. Such fluids can consist of gases, liquids, or combinations of gases, liquids and solids. An inevitable consequence is the internal maintenance of those pipelines. In the oil and gas industry this is done by using a pig (Pipeline Inspection Gauge). This is a cylindrical device which travels through the pipeline driven by the fluid flow, see for example Fig. 1. Pigs have a wide range of applicability, including cleaning the inside of a pipeline, removing excessive liquid from a liquid-gas pipeline, or distribution of corrosion inhibitor [1–4]. Pigs can also be equipped with intelligent sensors which can inspect the inner pipe wall [5], for example. There is a wide variety of pigs to perform these tasks. An example of three common utility pigs are (1) the mandrel pig, (2) the solid cast pig and (3) the foam pig, which are shown in Fig. 1 [1]. A mandrel pig consists of a metal core with elements mounted on this core. It depends on the purpose of the pigging operation which elements are mounted. Typical elements are scrapers for cleaning, guiding discs to ensure a proper alignment with the pipe and sealing elements to seal the pipe. These elements are normally made from polyurethane. A solid cast pig differs from a mandrel pig in the sense that it is made out of one material, often also polyurethane. A foam pig is made of softer material and has a larger volume. The pigging purpose and the costs determine which of the types is most appropriate to perform a pigging operation.

It is desirable that the product flow, which is driving the pigs through the pipeline, is interrupted as little as possible during the pigging operation. Conventional pigs, such as the ones displayed in Fig. 1a–c, typically completely seal the pipeline. As a consequence the speed of the device will be equal to the velocity of the product flow. However, often a lower travel speed is desired, as a too high pig velocity may damage the pig or pipeline. In addition, it has been shown that a lower pig velocity is also beneficial for the cleaning and inspection performance of the pig [3,7]. A solution to achieve a lower pig velocity while avoiding production deferment is the use of a by-pass pig, which does not seal the complete pipeline. Instead, a by-pass pig has a hole, or by-pass area, which allows fluid to by-pass the pig while it is moving inside the pipeline, see Fig. 1d. The presence of a by-pass will cause that the pig velocity is not dictated by the velocity of the product flow. Instead the pig velocity will be lower and it is now determined from a balance between the driving pressure force and the friction force between the pig and the pipe wall [8]. The risk, however, of using a by-pass pig is that the driving force on the pig becomes too low to overcome the wall friction force, which will result in a pig being stuck in the pipeline. To mitigate

* Corresponding author.
E-mail address: m.h.hendrix@gmail.com (M.H.W. Hendrix).

https://doi.org/10.1016/j.jprocont.2018.08.010
0959-1524/

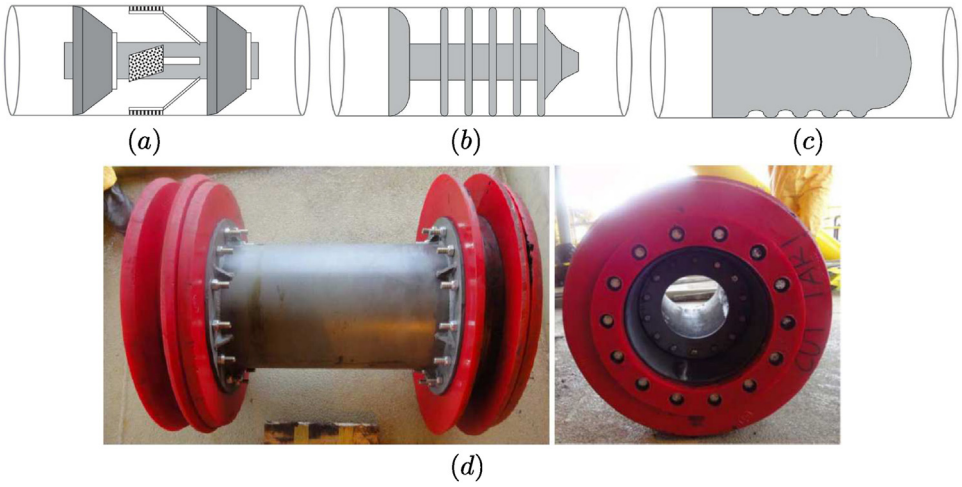

Fig. 1. Several pig types: (a) Mandrel pig. (b) Solid cast pig. (c) Foam pig. (d) By-pass pig. Adapted from [1,6].

the risk of a stuck pig, so-called speed controlled pigs have been designed which have an adjustable by-pass area which provides the right amount of by-pass such that the velocity of the pig is lowered, while the pig does not get stuck [7]. Detailed mechanisms on how such a control system should be designed are only scarcely found in literature [9,10].

In this paper we consider the movement of a pig in a low pressure gas-filled pipeline. Pigging of such low pressure gas-filled pipelines in actual field operation can lead to large oscillations in the pig velocity due to the compressibility of the gas, see for example [11,12]. This is because compressed gas pockets may build up at the upstream side of the pig when it is moving slower due to locally increased friction caused by for example irregularities in the inner pipe diameter. When the pressure in such a pocket has been sufficiently built-up, it is able to catapult the pig, resulting in large pig velocity excursions. This can lead to an unsafe and inefficient pigging operation. The effect described above gets more pronounced when the operating pressure or the flow velocity in the pipe is low. It can even result in a so-called 'stick-slip motion', where the pig slows down completely after a period of high velocity. This stick-slip motion of the pig is generally undesired in the industry. However, when a pig is equipped with appropriate speed control, the occurrence of high pig velocities in low pressure gas filled pipelines may be suppressed, which enables safe and effective pigging of these pipelines.

This paper is built up as follows. In Section 2 we first discuss the force balance on a (by-pass) pig. In addition we derive a simplified model which describes the motion of a pig in a low pressure system. The simplified model gives insights into the basic physical mechanisms which are key to unsteady pig motion due to low pressure conditions in gas filled pipelines. The simplified model relies on some assumptions, most notably the assumption that the pressure upstream of the pig is directly determined by the volume that the gas occupies upstream of the pig. In reality the pressure upstream of the pig will change as result of a transient pressure wave, rather than a instantaneous response to the change in volume. We therefore also include a more complete approach which models the motion of the pig in a transient 1D pipe model. In Section 3 we describe the experimental setup that has been used to perform pigging experiments. The experimental setup has been used in a previous work to test a prototype of a speed controlled pig [13,14]. In this work we more systematically study the behaviour of by-pass pigs with constant by-pass area which, in combination with the developed models, is expected to improve the design of such a speed controlled pig. In Section 4 a comparison will be made between the experimental results and the various models. The proposed models and experiments are subsequently used for the design of a PD controller in order to reduce pig velocity excursions through dynamically adjusting the size of the by-pass. Section 5 gives conclusions and discusses possibilities for future research.

2. Models

Whereas the pig velocity U_{pig} of a conventional pig in a pipeline is dictated by the bulk velocity U upstream of the pig, the pig velocity of a by-pass pig will be lower because part of the fluid is able to flow through the by-pass pig, see Fig. 2.

The motion of a by-pass pig in a horizontal pipeline is determined from a force balance between the driving pressure force F_p and frictional force F_{fric}. By applying a control volume analysis over the whole pig (including the by-pass area), F_p can be expressed as $F_p = \Delta p\, A$ where Δp is the pressure drop over the pig and A is the pipe cross-sectional area. The pressure drop is usually characterized by a pressure loss coefficient K defined as [15]:

$$K = \frac{\Delta p}{\frac{1}{2}\rho_{bp} U_{bp}^2}. \tag{1}$$

Here ρ_{bp} is the density of the fluid in the by-pass (which is taken as the density downstream of the pig) and U_{bp} is defined as the fluid velocity in the by-pass region taken relative to the pig velocity, see [16,8]. A mass balance taking into account a higher density upstream of the pig ρ_{up} due to compressibility of the fluid thus yields the following expression for U_{bp}:

$$U_{bp} = \frac{D^2}{d^2}\frac{\rho_{up}}{\rho_{bp}}(U - U_{pig}). \tag{2}$$

Here D is the pipe diameter and d the diameter of the by-pass hole. Substituting this expression for U_{bp} into Eq. (1) and applying a steady state force balance on the pig ($\Delta p\, A = F_{fric}$) results in an equation for the velocity of the by-pass pig [8,17]:

$$U_{pig} = U - \frac{d^2}{D^2}\frac{\rho_{bp}}{\rho_{up}}\sqrt{\frac{F_{fric}}{K\frac{1}{2}\rho_{bp}A}}. \tag{3}$$

When the by-pass area fraction d^2/D^2 goes to zero, Eq. (3) returns a pig velocity equal to the bulk velocity, as is the case for a conventional pig. When d^2/D^2 is not equal to zero, detailed knowledge of both K and F_{fric} are needed in order to accurately predict the pig velocity. The pig geometry in this research can be regarded as a

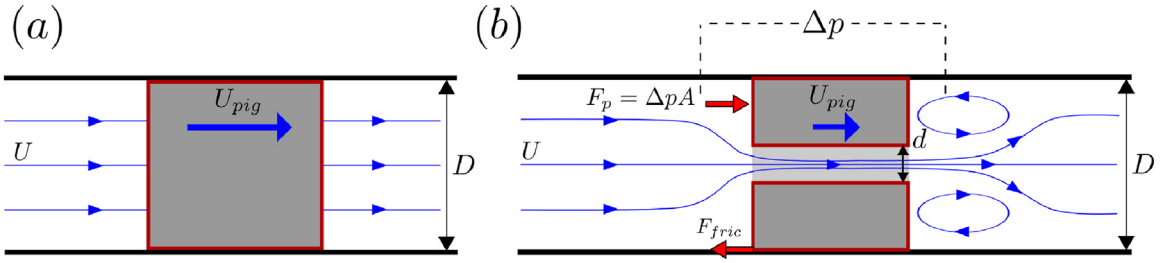

Fig. 2. Schematic motion of: (a) a conventional pig and (b) a by-pass pig.

thick orifice, for which the following correlation for the pressure loss coefficient has been proposed by Idelchik [15]:

$$K = 0.5\left(1 - \frac{d^2}{D^2}\right)^{0.75} + \frac{4fL_{pig}}{d} + \left(1 - \frac{d^2}{D^2}\right)^2. \tag{4}$$

Here L_{pig} denotes the length of the pig, and f is the Fanning friction coefficient which has been calculated using the Churchill correlation [18]. This correlation can be recognized as a combination of the loss associated with a sudden compression (first term), frictional loss in the by-pass (second term), and a sudden expansion (third term). This correlation has been extensively verified with simulations using CFD (Computational Fluid Dynamics) [8,19]. The loss coefficient for a by-pass pig that has a design different from a thick orifice geometry has been studied in [16]. Regarding the friction force F_{fric}, two main types of friction can be distinguished: (1) dry friction and (2) lubricated friction [20]. In case of lubricated friction (which obviously is only possible for twophase gas-liquid flow), a thin liquid layer is formed in between the two solids that is said to lubricate the relative motion. Such a lubrication layer normally reduces the friction coefficient considerably [21]. Our experiments are, however, carried out in a dry pipeline using air as working fluid. We model the dry sliding friction between the pig and the pipe wall with a constant coefficient. The proposed models of K and F_{fric} will be compared with experimental results which are described in Section 3. With F_p and F_{fric} in place, the equation of motion of the pig follows as:

$$m\frac{\mathrm{d}^2 s}{\mathrm{d}t^2} = F_p - F_{fric}. \tag{5}$$

Here m and s are the mass and the position of the pig, respectively.

We will now describe a simplified model and a more complete numerical model to describe the motion of a pig in a low pressure pipeline.

2.1. Simplified model

The simplified model considers the motion of the pig by modeling F_p as the force that results from the pressure in the gas pockets on both sides of the pig. It is assumed that the pressure in these pockets is uniform and adapts instantaneously to any changes in the volume that they occupy. The pressure upstream p_{up} of the pig thus reads

$$p_{up} = \frac{p^*}{\rho^*}\rho_{up} = \frac{p^*}{\rho^*}\frac{M_{tot}}{As} = \frac{p^*}{\rho^*}\frac{M_0 + \dot{M}t}{As}. \tag{6}$$

Here the ideal gas law is used to relate the pressure in the upstream pocket to the upstream density ρ_{up}, using $p^* = 101\,\mathrm{kPa}$ and $\rho^* = 1.2\,\mathrm{kg/m^3}$ as reference values for air. Furthermore, M_{tot} denotes the total mass in the upstream pocket, A is the pipe cross-sectional area, and s is the location of the pig as measured from the inlet. The total mass M_{tot} is a sum of the initial mass M_0 at $t = 0$ and the (constant) mass flux at the inlet $\dot{M}$ multiplied by the time t (Fig. 3).

Applying the same approach to the downstream side of the pig leads to a constant pressure $p_{down} = p_{out}$ for the downstream gas pocket. This approach effectively neglects frictional pressure losses. Substituting $F_p = A(p_{up} - p_{down})$ into Eq. (5) yields:

$$m\frac{\mathrm{d}^2 s}{\mathrm{d}t^2} = \frac{p^*}{\rho^*}\frac{M_0 + \dot{M}t}{s} - Ap_{out} - F_{fric}. \tag{7}$$

The equilibrium position $s(t) = s_{eq}(t)$ can be found by setting the left hand side of Eq. (7) equal to zero, which gives:

$$s_{eq}(t) = \frac{p^*}{\rho^*}\frac{M_0 + \dot{M}t}{Ap_{out} + F_{fric}}. \tag{8}$$

The equilibrium velocity v_{eq} can be found by differentiating Eq. (8), which yields:

$$v_{eq} = \frac{p^*}{\rho^*}\frac{\dot{M}}{Ap_{out} + F_{fric}}. \tag{9}$$

We now define $s(t) = s_{eq}(t) + \delta s(t)$. Dividing Eq. (7) by $Ap_{out} + F_{fric}$ and substituting the decomposition of s into Eq. (7) yields

$$\frac{m}{Ap_{out} + F_{fric}}\frac{\mathrm{d}^2\delta s}{\mathrm{d}t^2} = \frac{s_{eq}(t)}{s_{eq}(t) + \delta s} - 1. \tag{10}$$

Assuming that the perturbations of δs are small ($\delta s \ll s_{eq}$) we can expand the first term on the right hand side of Eq. (10):

$$\frac{m}{Ap_{out} + F_{fric}}\frac{\mathrm{d}^2\delta s}{\mathrm{d}t^2} = -\frac{\delta s}{s_{eq}(t)}. \tag{11}$$

Eq. (11) can be solved analytically (see Appendix A), yielding an explicit expression for $\delta s(t)$:

$$\delta s(t) = C_1 k \mathrm{J}_1(2k) - C_2 k \mathrm{Y}_1(2k). \tag{12}$$

Here J_1 is the Bessel function of the first kind with order 1 and Y_1 is the Bessel function of the second kind with order 1. Futhermore $k(t)$ is given by:

$$k(t) = \omega(t)\left(\frac{M_0}{\dot{M}} + t\right), \tag{13}$$

where $\omega(t)$ is given by:

$$\omega(t) = \sqrt{\frac{\left(Ap_{out} + F_{fric}\right)}{s_{eq}(t)\,m}}. \tag{14}$$

Differentiating Eq. (12) yields an expression for the perturbed velocity δv (see Appendix A):

$$\delta v(t) = \omega^2(t)\left(\frac{M_0}{\dot{M}} + t\right)\left(C_1 \mathrm{J}_0(2k) - C_2 \mathrm{Y}_0(2k)\right). \tag{15}$$

C_1 and C_2 are integration constants (with unit length) which can be found from the initial conditions for δs and δv. This approximate analytic expression will be compared with numerical integration of Eq. (7) in section 4.3.

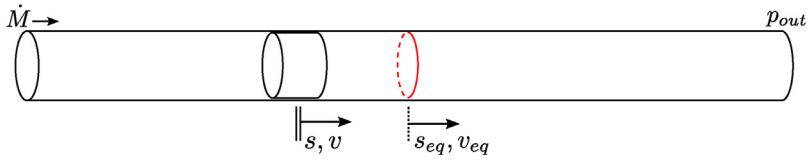

Fig. 3. Schematic motion of simplified pig model.

2.1.1. Local analysis

When fixating the value for s_{eq}, Eq. (11) can be recognized as the equation which describes a harmonic oscillator, for which the solution is given as:

$$\delta s(t) = C_3 \sin(\omega t + C_4). \tag{16}$$

Here ω is the local frequency of the solution for a given s_{eq}, as given by Eq. (14), and C_3 and C_4 are integration constants. The maximum value for $\delta v_{\max}$ can be found by differentiating Eq. (16) and determining the maximum which gives:

$$\delta v_{\max} = C_3 \omega. \tag{17}$$

The value of C_3 (and C_4) is determined by the initial conditions for $\delta s(t=0)$ and $\delta v(t=0)$, which we denote δs_0 and δv_0 respectively. C_3 can then be determined as:

$$C_3 = \frac{\sqrt{\omega^2 \delta s_0^2 + \delta v_0^2}}{\omega}. \tag{18}$$

Substituting this expression for C_3 into Eq. (17) gives:

$$\delta v_{\max} = \sqrt{\omega^2 \delta s_0^2 + \delta v_0^2} = \sqrt{\frac{A p_{out} + F_{fric}}{s_{eq} m} \delta s_0^2 + \delta v_0^2}. \tag{19}$$

In order to determine δs_0 and δv_0 and s_{eq} we now consider a pig which moves in a stick-slip fashion and just enters the slip phase. In this analysis we introduce the static friction force $F_{fric,s}$, which is usually higher than the value of the sliding dynamic friction force F_{fric}. We now consider a pig that sticks at a location $L = s_{eq} + \delta s_0$. Just at the point before the pig starts slipping ($t=0$) a force balance can be constructed which reads:

$$(p_{up} - p_{out})A = \left(\frac{p^*}{\rho^*}\frac{M_0}{AL} - p_{out}\right) A = F_{fric,s} \tag{20}$$

This equation can be solved for M_0 and the result can be substituted into Eq. (8) to yield an expression for the equilibrium position s_{eq}:

$$s_{eq} = \frac{L(F_{fric,s} + p_{out}A)}{F_{fric} + p_{out}A}. \tag{21}$$

Using $\delta s_0 = L - s_{eq}$ and $\delta v_0 = -v_{eq}$ and substituting these expressions into Eq. (19) gives the following expression for the maximum velocity $v_{\max}$ which occurs during the stick-slip cycle:

$$v_{\max} = v_{eq} + \delta v_{\max} = v_{eq} + \sqrt{\frac{L(F_{fric,s} - F_{fric})^2}{m(F_{fric,s} + p_{out}A)} + v_{eq}^2}. \tag{22}$$

We note that if the static friction force $F_{fric,s}$ equals the dynamic friction force F_{fric} the maximum velocity is simply equal to twice the upstream equilibrium velocity v_{eq}.

2.2. Full numerical model

The full numerical model discretizes the fluid domain into multiple finite volumes, rather than describing the fluid upstream and downstream of the pig as one pocket as was done in the model described in Section 2.1. The resulting model is a one-dimensional (1D) transient model, which solves for cross-sectionally averaged quantities such as pressure and velocity as function of the pipe coordinate s, which runs along the pipe, and time t. Examples of 1D transient tools which are used in the oil and gas industry to model pig motion in a pipeline include OLGA and LedaFlow [22,23]. The current 1D model relies on the 1D extended Euler equations from which the cross-sectionally averaged mass and momentum equation read:

$$\frac{\partial}{\partial t}(\rho A) + \frac{\partial}{\partial s}(\rho u A) = 0, \tag{23}$$

$$\frac{\partial}{\partial t}(\rho u A) + \frac{\partial}{\partial s}(\rho u^2 A + pA) = -\tau(\pi D). \tag{24}$$

Here τ is the wall shear stress which is calculated as:

$$\tau = \frac{1}{2}\rho u^2 f, \tag{25}$$

where f is the Fanning friction coefficient calculated using the Churchill relation [18]. As in the simplified model, we calculate $\rho = \rho(p)$ through the ideal gas law, that is $\rho = (\rho^*/p^*)p$. Eqs. (23) and (24) form a closed system of equations which is discretized using the finite volume method on a staggered grid, see Fig. 4.

Conservation of mass (Eq. (23)) is discretized on the p-volume Ω_p, in which p is defined at the center of the volume:

$$\frac{\mathrm{d}}{\mathrm{d}t}\left(\rho_i \Omega_i^p\right) + \rho_{i+1/2} u_{i+1/2} A - \rho_{i-1/2} u_{i-1/2} A = 0 \tag{26}$$

Here $\Omega_i^p = A\Delta s_i = A(s_{i+1/2} - s_{i-1/2})$ is the size of the finite p-volume. Conservation of momentum (Eq. (24)) is discretized in a similar way:

$$\frac{\mathrm{d}}{\mathrm{d}t}\left(\rho_{i+1/2} u_{i+1/2} \Omega_{i+1/2}^u\right) + \rho_{i+1}(u_{i+1})^2 A - \rho_i (u_i)^2 A = -\tau_{i+1/2}(\pi D)\Delta s_{i+1/2} \tag{27}$$

Here $\Omega_{i+1/2}^u = A\Delta s_{i+1/2} = A(s_{i+1} - s_i)$ is the size of the finite u-volume. Some terms in Eqs. (26) and (27) require interpolation. If the term is part of a convective term a flux limiter is used, otherwise central interpolation is used. The system is integrated in time using the second order BDF2 scheme. For more details the reader is referred to [24].

2.2.1. Regridding

The pig is implemented as a moving border of a finite volume. As a consequence, the finite volume in front of the pig will reduce in size and the finite volume at the back of the pig will increase in size. We solve our system of equations in conservative form, which means that we solve for the total mass $U_{mass,i} = \rho_i \Omega_i^p$ and total momentum $U_{mom,i+1/2} = \rho_{i+1/2} u_{i+1/2} \Omega_{i+1/2}^u$. Since the size of the finite volume is part of the conservative variable $U_{mass,i}$ and $U_{mom,i+1/2}$, the change of the size of the finite volume due to the motion of the pig is naturally captured. The pig motion is solved by applying Newton's second law, Eq. (5). The pig position and pig velocity are appended to the vector of unknowns which contains $U_{mass,i}$ and $U_{mom,i+1/2}$ for each finite volume. The resulting system of equations is solved in a monolithic fashion. Since the pig position and pig velocity are part of the solution, there always exists a mapping of U_i to the primitive variables u_i and ρ_i.

As a result of the current implementation the finite volume in front of the pig will at some point become too small, whereas the

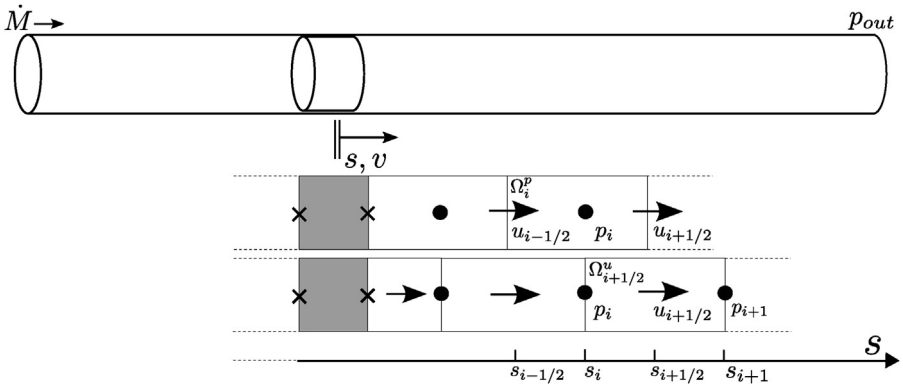

Fig. 4. Staggered grid layout in the full numerical model.

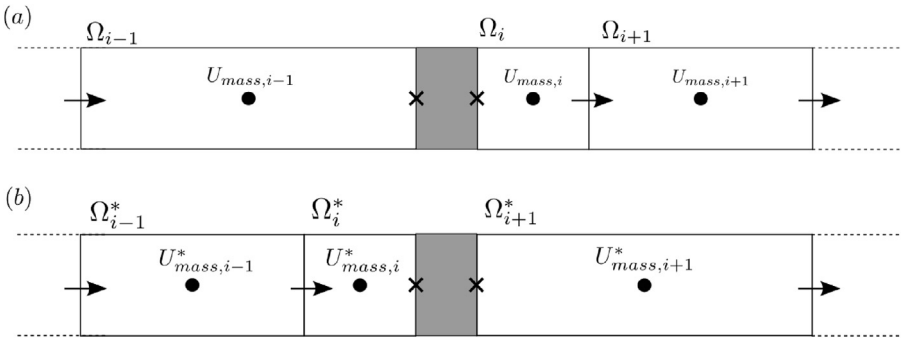

Fig. 5. Grid regeneration. (a) Grid before regeneration. (b) Grid after regeneration.

finite volume at the back of the pig will become too large. Therefore, the grid has to be regularly regenerated as the pig traverses through the pipe. We perform the grid regeneration as follows. When the finite volume cell in front of the pig gets smaller than half the size of a cell as found in the interior, it will be merged with its neighbouring cell. Similarly, if the cell at the back of the pig gets larger than 1.5 the size of a cell as found in the interior, it will be split up in two cells, see Fig. 5. The conservative variable U_i will be reconstructed accordingly. The mass $U^*_{mass,i}$ of the volume in front of the pig after regenaration is determined by the sum of the masses of the cells before merging, see Fig. 5:

$$U^*_{mass,i+1} = U_{mass,i} + U_{mass,i+1} \tag{28}$$

The mass of the cells at the back of the pig is distributed proportionally to the size of the newly created cells:

$$U^*_{mass,i-1} = \Omega^*_{i-1} U_{mass,i-1} / \Omega_{i-1} \tag{29}$$

$$U^*_{mass,i} = \Omega^*_{i} U_{mass,i-1} / \Omega_{i-1} \tag{30}$$

The merging and splitting of momentum cells $U_{mom,i+1/2}$ is performed in the same way.

3. Experimental setup

A schematic of the flow loop in which the laboratory experiments are conducted is depicted in Fig. 6a. The loop consists of a horizontal transparent perspex pipe with a length of 62 m and an internal diameter of 52 millimeter. The experiment is operated in single phase using air as working fluid. The flow loop is equipped with a pig launcher located at the inlet of the loop that allows to insert a pig into the system, see Fig. 6b. By placing the pig in the launcher and subsequently redirecting the air through the launcher the pig will be inserted into the pipe. After traversing along the pipe the pig is trapped at the outlet and can be retrieved. Fig. 6c shows a close-up of one of the pigs that is used in the experiments.

The air that is used as working fluid in the experiment is tapped from an air supply system which is kept at a pressure of 8 bar. A pressure reducing valve brings this down to 2 bar. The air then passes through a gas flow meter (Bronkhorst – MASS-STREAM Series D-6300) where the air mass flux can be controlled. The flow loop is equipped with two pressure sensors (Validyne DP15), see Fig. 6a. The average pig velocity is computed as the total length divided by the residence time. For the length, the distance between the upstream pressure transducer and the pig receiver (i.e. the flow loop exit) is used, which amounts a distance of 62 m. The residence time is the time difference found by studying the pressure increase and decrease measured by the upstream pressure transducer. In addition, the pressure drop that is measured over the pig allows to determine the frictional force of the pig with the pipe wall, since in steady state the driving pressure force and the frictional force must balance, see Eq. (5). Three synchronized high speed cameras (GoPro HERO4) located at about 41.5 m downstream of the first pressure sensor allow for the local dynamics of the pig to be analyzed, see Fig. 6a. The cameras are operated at a framerate of 120 frames per second at a resolution of 720p. The cameras are separated in such a way that their field of views partly overlap. The three images of each camera are stitched together during post-processing using a cross-correlation algorithm in order to construct one single image. The total field of view thus obtained is 7.5 m. The cameras are synchronized in time by using a flash light as reference point which is visible on all three cameras at the beginning of a measurement.

The pigs are custom-made and have a flexible modular design which allows for the by-pass area and sealing disks to be easily interchanged. The sealing disk makes sure that no fluid leaks between the pig and the pipe wall, and that the only fluid that flows through the pig goes through the by-pass area, see Fig. 6c. The by-pass area is formed by a concentric hole in the centre of the

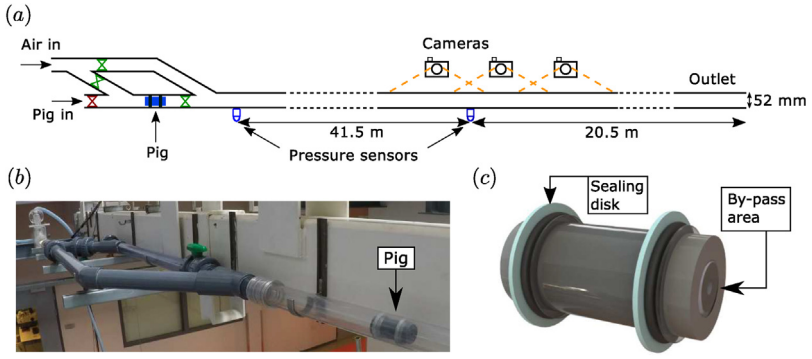

Fig. 6. (a) Overview of the flow loop. (b) Close-up of the pig launcher. (c) Drawing of the pig.

Table 1
Properties of pig configurations.

Property	Configuration 1	Configuration 2	Unit
Material sealing disk 1	EPDM	Para rubber	–
Hardness sealing disk 1	35[a]	45	Shore A
Outer diameter sealing disk 1	57	57	mm
Thickness sealing disk 1	4	2	mm
Material sealing disk 2	EPDM	EPDM	–
Hardness sealing disk 2	35	35	Shore
Outer diameter sealing disk 2	55	48	mm
Thickness sealing disk 2	4	4	mm
Average friction	25.68	41.3	N

[a] The hardness is measured according Shore 00 standards. A comparable Shore A value is given here to compare with the other material.

pig body and ranges from 0% to 4% of the total cross-sectional area in the current experiment.

Two pig configurations have been tested: configuration 1 and configuration 2, see Fig. 7a and b respectively. Both configurations have a sealing disk with a slightly larger diameter than the inner pipe diameter. The difference in the diameters, or the oversize, ensures that the pig properly seals the pipeline and that no leakage occurs between the pig and the pipe wall [1].

The two pig configurations have a different sealing disk compression behaviour. The seals in configuration 1 are compressed in the radial direction. For industrial pigs, sealing disks deformed in a similar way are referred to as scraper disks [1]. Since the used material of our small-scale pigs is rather flexible, the variation in friction due to diameter variations is limited. Furthermore, the clamping disks can be relatively large which prevents tilting of the pig. A downside of the flexible seals is that severe wear of the sealing disks can occur. In the current experiment they were therefore replaced after roughly every 6 runs. The seals in configuration 2 have more space to bend compared to configuration 1. This is comparable with what in industry is referred to as cone disks [1]. The sealing disk material of configuration 2 is much harder and shows very good wear properties. A downside is that more space is required for the seals to bend, which increases the chance that the pig is being tilted. The dimensions of pig configurations 1 and 2 are displayed in Fig. 7c and d respectively. More details on the material and sizes of the sealing disks are listed in Table 1. To build up sufficient pressure, it is essential that the pig properly seals the pipe. Cell rubber (EPDM) with a closed cell structure is chosen for configuration 1 to guarantee that the sealing disk is impermeable. Para rubber is used for configuration 2, which has very good wear properties.

From the pressure measurements during the pigging runs an estimation of the friction was obtained for both configurations, see Table 2. This table will be explained in more detail in the next section.

Table 2
Properties of pig configurations.

	By-pass area ratio(%)			
	0	1	2	4
Configuration 1				
Average friction (N)	27.1 ± 6.5	25.5 ± 3.0	23.9 ± 5.0	26.5 ± 4.5
Configuration 2				
Average friction (N)	40.3 ± 1.5	44.4 ± 2.9	39.5 ± 2.5	NA

4. Results

This section starts with some overall results from the various pigging runs that have been conducted in the lab facility. In total 72 runs were used in the analysis of configuration 1, and 60 runs were performed with configuration 2. The overall quantities include the average pig velocity and the required driving pressure for various by-pass pigs. These results are important for verifying steady state by-pass pigging models which can be used to predict the pig velocity. In addition, the results are relevant for 1D transient models in which the trajectory of the pig can be monitored [22,23]. These 1D transient models rely on accurate correlations to model the pig dynamics. Subsequently, Section 4.2 presents an analysis of the local pig dynamics which gives insight in the oscillatory behaviour of the pig motion due to the low pressure conditions. A comparison with the models developed in Section 2 will be made. The results for the local behaviour of the pig motion are used in Section 4.3 to design a simple PD controller to reduce the velocity excursions of the pig by dynamically adjusting the by-pass area.

4.1. Overall behaviour

For each pigging run the pressure from the upstream and downstream pressure sensors is recorded. Fig. 8a shows a typical signal that is obtained. Here the mass inflow rate is $\dot{M} = 0.0089$ kg/s, and the pig has configuration 2 with 0% by-pass. When the pig traverses along the upstream pressure sensor the excess pressure increases to about 20 kPa. After traversing 41.5 m the pig reaches the downstream pressure sensor, which is clearly visible by the uptake of the signal at around 29 s. When the pig reaches the outlet of the pipe both signals drop because the pressure that was built up behind the pig is now released.

From the time difference between the instant that the pig reaches the upstream pressure sensor and the outlet, the average pig velocity can be obtained. In addition, the average driving pressure force needed to propel the pig can be deduced from the measurements, which in steady state balances the friction force between the pig and the pipe wall. Fig. 8b and c shows the average driving pressures ($\tilde{p}_{up} - \tilde{p}_{down}$) as function of the pig velocity for configuration 1 and for configuration 2, respectively. The measure-

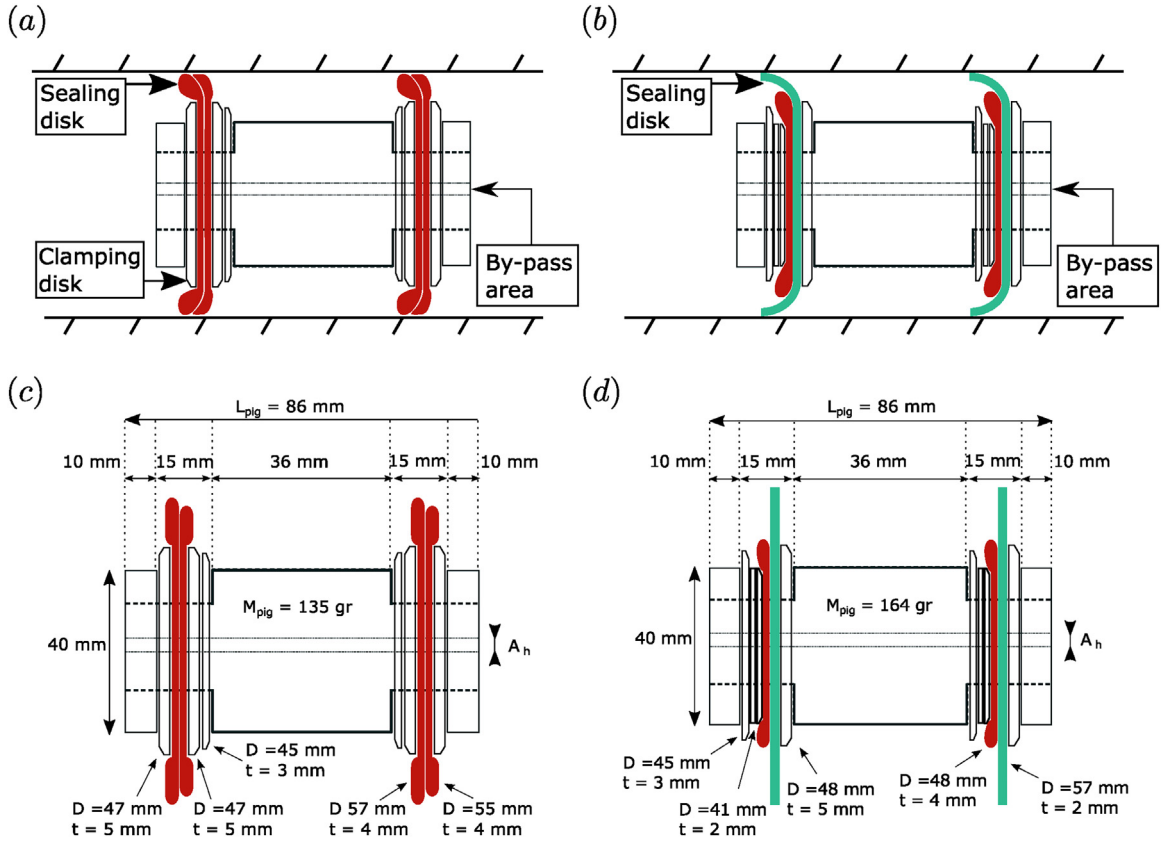

Fig. 7. (a) Schematic of pig configuration 1. (b) Schematic of pig configuration 2. (c) Detailed geometry of pig configuration 1. (d) Detailed geometry of pig configuration 2.

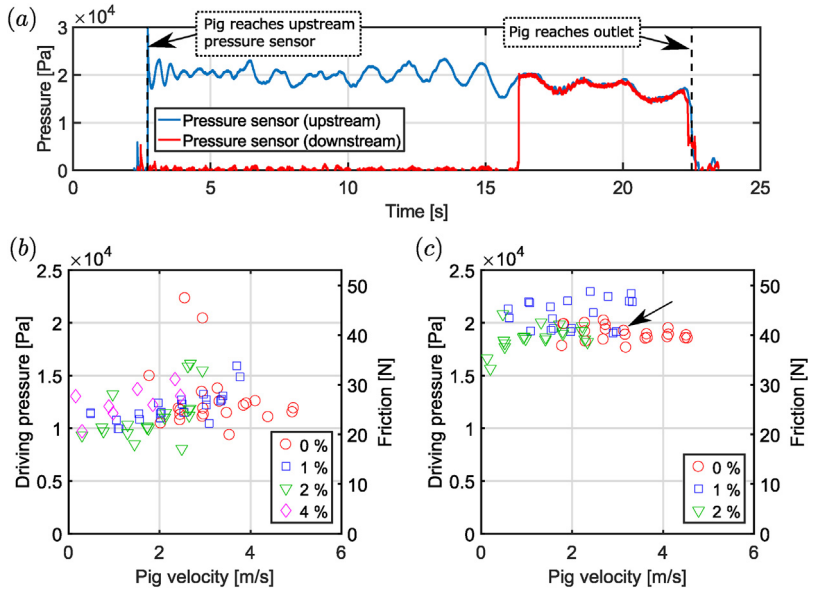

Fig. 8. (a) Pressure signal for configuration 2 with 0% by-pass. (b) Average driving pressures for the configuration 1 pigging runs. (c) Average driving pressures for the configuration 2 pigging runs. The symbols in (b) and (c) denote various by-pass ratios.

ment corresponding to the pressure signal displayed in Fig. 8a is indicated by the black arrow in Fig. 8c. The different pig velocities have been obtained by varying both the upstream bulk velocity of the air as well as the by-pass area, as will be explained in more detail below. When inspecting Fig. 8b and c, we note that the driving pressure is not a function of the pig velocity. This substantiates our earlier modeling assumption that the friction of the pig can indeed be approximated by a constant (dry) friction force within the current parameter range. It is important to note that this can be different when the transported fluid is a liquid instead of a gas or when there is two-phase gas-liquid flow, due to the effect of possible lubrication. From the data presented in Fig. 8 the overall average friction force for each by-pass pig (0, 1, 2, and 4%) for the two configurations can be obtained. These average friction values, with the standard deviation, are summarized in Table 2. As can be noted from both Fig. 8 and Table 2 no runs for a by-pass of 4% were

performed for configuration 2. The reason is that the friction of this pig with 4% by-pass is too high which results in a stalled pig.

One of the main reasons for using by-pass pigs is the ability to reduce the pig velocity. The flow velocity can be kept at the nominal production rate whereas the pig travels through the pipeline at a lower velocity. The reduction in the pig velocity depends on the by-pass ratio, see Eq. (3). Fig. 9 shows the pig velocity versus the flow velocity for both configurations 1 and 2. Different colours and symbols are used for different by-pass area ratios.

The red circles represent the pigging runs with zero by-pass. These pig velocities should be equal to the upstream bulk velocity, which is indicated by the 45 degree line in gray. The results for both configurations indeed follow this line. The other markers represent the pig velocity for a specific by-pass ratio. As can be noted an increase in by-pass area does indeed result in a reduction of the pig velocity. It can be deducted from Fig. 9 that the reduction in pig velocity is around 1 m/s for each percentage of by-pass area that is added relative to the zero by-pass case. For a more quantitative comparison with theory we compare the experimental results with the velocity predicted by Eq. (3), which is shown by the black line. In this equation the friction force F_{fric} is taken equal to the average measured value of the friction, see Table 2. The value for K in Eq. (3) is modeled by the Idelchik relation (Eq. (4)) to model the pressure drop. Therefore the solid line effectively plots the predicted travel velocity based on the Idelchik relation and a constant predetermined friction. In addition the velocity calculated based on plus and minus the standard deviation of the friction force are included as black dashed lines. As was already shown in Table 2, the spread is higher for configuration 1. Fig. 9 shows very good agreement between the measurements and the values based on the Idelchik relation. During the pigging runs oscillatory motion of the pig was observed, which will be discussed in the next section. These results show that even though Eq. (3) is based on a steady state balance it can be applied to unsteady pig motion from which an average pig velocity is extracted. We further note that the point where the black line intersects the horizontal axis indicates a minimum average bulk velocity which is needed to propel the by-pass pig. Below this bulk velocity not enough driving pressure is generated to overcome the average friction force of the pig with the pipe wall. Note that in practice the minimum required bulk velocity may be higher as the black line is based on an average friction. A local increase in friction, for example due to irregularities in the pipe diameter, may cause a pig to stall even above this velocity. In the next section we will discuss the local behaviour which is observed by analyzing detailed dynamics of the pig motion as well as time series of the upstream pressure.

4.2. Local behaviour

We now focus on the local behaviour of the pig motion. As was mentioned in the previous section stick-slip motion was observed in the experiment. The oscillatory signal of the pressure (Fig. 8a) indicates that the pressure upstream of the pig is indeed not constant as would be expected in case the pig would move at a constant steady state velocity. Fig. 10 shows the upstream pressure signal which is displayed in Fig. 8a together with a prediction from the simplified model, as described in section 2.1. The model is initiated at two time instances: $t_1 = 3.04$ and $t_2 = 12.20$ s. These instances are selected as case examples in the time series of the upstream pressure, as a clear oscillatory signal is visible, see Fig. 10. In order to evaluate the simplified model to predict the upstream pressure, Eq. (6) is used. To evaluate Eq. (6) the initial position of the pig needs to be known. Clearly, the pig is located further downstream at $t = t_2$ than at $t = t_1$. To determine the initial pig positions for these two cases, the equilibrium velocity (Eq. (9)) is multiplied by the traveling time t_1 and t_2. Furthermore, the dynamic friction force F_{fric} and the static friction force $F_{fric,s}$ are input parameters to the model. F_{fric} has been estimated by determining the mean driving pressure which is needed to propel the pig multiplied by the pipe area, as has been described in section 4.1. $F_{fric,s}$ is estimated at 1.5 times the standard deviation of the pressure signal of the upstream pressure sensor multiplied by the pipe area. This leads to $F_{fric} = 40.80$ N and $F_{fric,s} = 43.87$ N. The pressure values which are needed to balance the friction forces F_{fric} and $F_{fric,s}$ are indicated with a dashed and a dotted line respectively, see Fig. 10.

Fig. 10 shows qualitatively good agreement between the measured upstream pressure and the value obtained with the simplified model. Both the model and the measurements show that the frequency of the oscillation decreases when the pig moves further through the pipeline. This is in line with Eq. (14), which describes the local frequency of the oscillation. It must be noted that the simplified model idealizes the model of the friction in the sense that it assumes one value of the static friction $F_{fric,s}$ and one value of the dynamic friction F_{fric}. In reality the value of $F_{fric,s}$ may vary due to for example irregularities in the inner pipe diameter. Nonetheless it can be observed that the frequency of oscillations of the pig motion can be captured by the model by estimating constant values for F_{fric} and $F_{fric,s}$.

The oscillation in pressure which was discussed above is directly connected to oscillations in the pig velocity. We now use the images from the high speed cameras, which are located around 41.5 m downstream of the upstream pressure sensor (see Fig. 6), to investigate the maximum pig velocity that occurs. The maximum velocity is found from the video recordings by tracking the location of the pig using image processing, as discussed in Section 3. The experiments performed with configuration 2 are selected, because the spread in average friction is smaller compared to configuration 1, see Section 4.1. The results are shown in Fig. 11a. The coloured symbols represent the different by-pass pigs that are used in the experiment. In addition the maximum velocity as predicted by the simplified model, Eq. (22), is shown. Here the dynamic friction F_{fric} is taken equal to the value of the 0% by-pass pig, which is 40.3 N, see Table 2. The static friction $F_{fric,s}$ is taken equal to 40.3 N, 44 N, and 48 N, as shown by the solid, dashed, and dotted line, respectively. It is clear from Fig. 11a that a higher value of $F_{fric,s}$ promotes a higher maximum pig velocity. This is explained by the higher pressure in the gas pocket upstream of the pig corresponding to the higher value of the static friction force $F_{fric,s}$. The black solid line represents the maximum pig velocity in case $F_{fric,s}$ is equal to F_{fric}. According to Eq. (22) this corresponds to a maximum pig velocity which is twice the average pig velocity. From the measurements it is clear that the maximum pig velocity is indeed significantly higher than the average travel velocity of the pig as most of the measurements are located at the left of the solid line. In addition to the measurements and the simplified model, the results of the full numerical model as explained in Section 2.2 are included for the three different values of $F_{fric,s}$ (lines with solid black circles). The by-pass in this simulation is set equal to 0%. The maximum pig velocity has been obtained from a simulation in which the pig is inserted 40 m downstream. This location ensures that the maximum velocity occurs within the location corresponding to the field of view of the cameras in the experiment. Grid converged solutions were typically obtained when using a total of 200 finite volumes, which corresponds to a computational cell length of about 0.34 m, and a timestep of 0.0025 s.

When comparing the results of the simplified model with the full numerical model and the experimental data we note that the simplified model overpredicts the maximum velocity. This is due to the assumption in the simplified model that the influence of pressure waves due to the acceleration of the fluid around the pig are negligible. The full numerical model does incorporate this, and therefore predicts a lower maximum velocity within this parameter

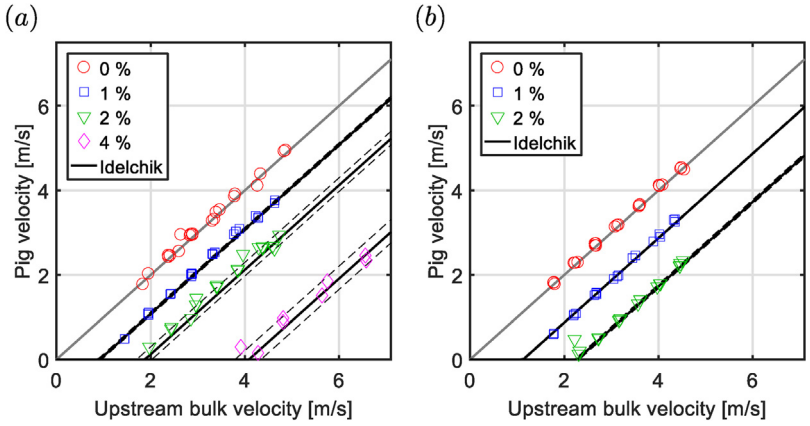

Fig. 9. Pig velocity as function of upstream bulk velocity (a) Configuration 1, (b) Configuration 2. The dashed lines denote the standard deviation in the calculated pig velocity.

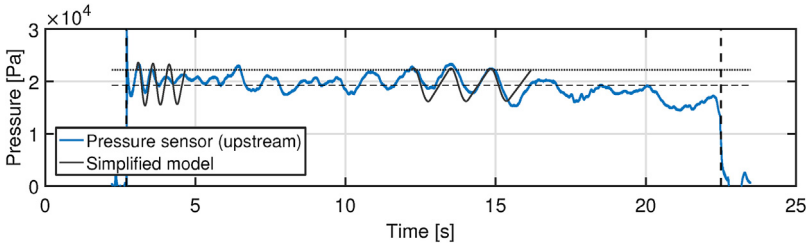

Fig. 10. Pressure signal for configuration 2 with 0% by-pass compared with the simplified model. The horizontal dashed lines represent the average pressure plus and minus 1.5 times the standard deviation of the pressure multiplied by the pipe area.

range. The effect of these pressure waves compared to the overall pressure drop over the pig becomes less important if the friction force of the pig is larger. To test this hypothesis we run the same simulation, but now increase the value of F_{fric} by a factor 10 to F_{fric} = 403 N. Again three values of $F_{fric,s}$ have been chosen as 403 N, 422 N, and 440 N. We also increased the pig mass by a factor 10. We now see that the agreement between the simplified model and the full numerical model is much closer. Therefore we conclude that the simplified model can be used to estimate the maximum velocity if the magnitude of the pressure waves that occur in the fluid due to the acceleration of the pig are negligible compared to the pressure drop over the pig.

Fig. 11a shows the simplified model (lines) and the full numerical model (lines with solid black circles) evaluated for the 0% by-pass case. The experimental results performed with the 1% and 2% by-pass pigs are superimposed in the plot. Although the travel velocity of the by-pass pigs is lower, it can be noted that the results with 1% and 2% by-pass follow the trend of the results with 0% by-pass and thus have a significantly higher maximum velocity than the average travel velocity. We also have evaluated the simplified model by incorporating a by-pass. To make the simplified model suitable for by-pass pigs, Eq. (7) is modified to take into account the mass leakage that occurs through the by-pass:

$$m\frac{\mathrm{d}^2 s}{\mathrm{d}t^2} = \frac{p^*}{\rho^*}\frac{M_0 + \dot{M}t - \int \dot{M}_\beta \mathrm{d}t}{s} - Ap_{out} - F_{fric}, \tag{31}$$

where $\dot{M}_\beta$ is the mass flux through the by-pass given by

$$\dot{M}_\beta = (U - U_{pig})A\rho_{up}. \tag{32}$$

Here U can be solved from Eq. (3) for a given mean pig velocity U_{pig}. Instead of constructing an analytical solution, which was possible for 0% by-pass case, Eq. (31) is solved numerically. As an example the results for $F_{fric,s}$ = 48 N are included in Fig. 11a with white squares and white triangles for 1% and 2% by-pass respectively. These symbols closely follow the line of the simplified model corresponding to 0% by-pass. It can thus be concluded that a fixed by-pass area does not reduce the velocity excursion of the pig. This is also confirmed by the experimental results as shown in Fig. 11: although the average speed of the by-pass pigs is lower, the maximum velocity is still significantly higher than the average pig velocity. However when the by-pass area is not fixed, but instead is adjusted dynamically, the maximum pig velocity can be reduced, which will be discussed in the next section.

4.3. Control

In the previous sections the mechanism behind oscillatory motion of a pig in a low pressure pipeline has been explained and described. Due to stick-slip behaviour it was found that the maximum pig velocity is significantly higher than the average pig velocity for both conventional pigs (i.e. no by-pass) as well as pigs with by-pass. We now propose a control mechanism which relies on actively regulating the size of the by-pass, such that part of the pressure in the gas pocket upstream of the pig can be released. This would result in a lower maximum pig velocity, as the driving upstream pressure is reduced during the acceleration of the pig. It is important to note that if the by-pass stays open too short or too little, not enough pressure is released and the pig still accelerates to a high velocity. On the other hand, if the by-pass stays opens too long, too much pressure is released and instead of mitigating the spike in pig velocity, a new stick-slip cycle is promoted. The ideal by-pass opening can be determined by an appropriate control algorithm. The time scale on which the controller should act is given by $2\pi/\omega$, where ω is the local angular frequency of the oscillation, given by Eq. (14). We will now demonstrate a simple controller based on the physical models that have been formulated, which set some minimum requirements for the design of a controller. There-

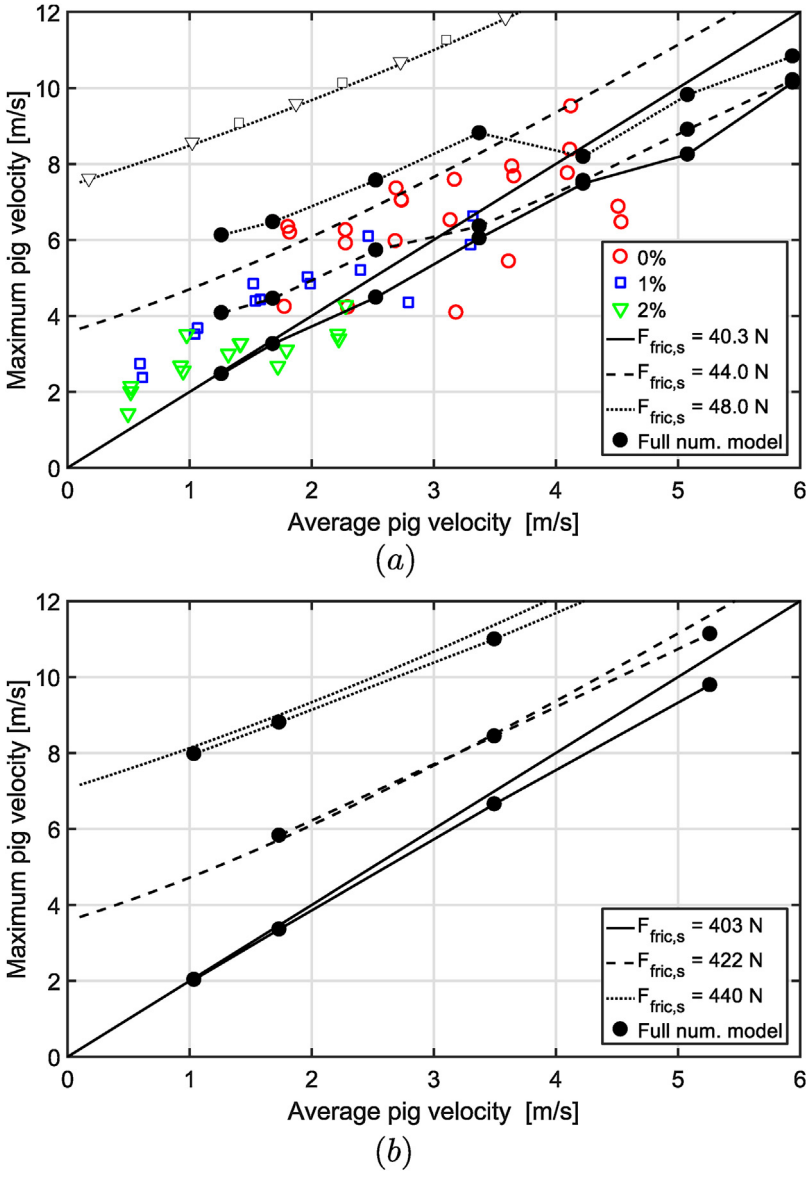

Fig. 11. Maximum pig velocity versus average pig velocity; (a) Experimental conditions. (b) Higher friction (10 times) compared to experimental conditions.

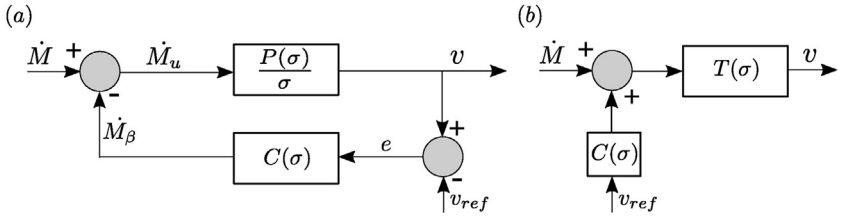

Fig. 12. (a) Feedback loop. (b) Equivalent feedback loop with closed loop transfer function $T(\sigma)$.

fore we again consider a pig that sticks at location L at $t=0$. When defining $\tilde{s} = s - L$ and $\tilde{v} = \mathrm{d}\tilde{s}/\mathrm{d}t$ we can write Eq. (31) as:

$$m\frac{\mathrm{d}^2\tilde{s}}{\mathrm{d}t^2} = \frac{p^*}{\rho^*}\frac{M_0 + M_u}{\tilde{s} + L} - Ap_{out} - F_{fric}. \tag{33}$$

Here $M_u = \int_0^t (\dot{M} - \dot{M}_\beta)\mathrm{d}t$ is the upstream mass that has been added after the pig starts moving. We can put Eq. (33) in state space form by selecting M_u as control variable and linearizing around the point $\tilde{s} = 0, \tilde{v} = 0, M_u = 0$:

$$\begin{bmatrix} \dot{\tilde{s}} \\ \dot{\tilde{v}} \end{bmatrix} = \begin{bmatrix} 0 & 1 \\ -\frac{p^* M_0}{\rho^* L^2 m} & 0 \end{bmatrix} \begin{bmatrix} \tilde{s} \\ \tilde{v} \end{bmatrix} + \begin{bmatrix} 0 \\ \frac{p^*}{\rho^* L m} \end{bmatrix} M_u = \begin{bmatrix} 0 & 1 \\ -\omega^2 & 0 \end{bmatrix} \begin{bmatrix} \tilde{s} \\ \tilde{v} \end{bmatrix} + \begin{bmatrix} 0 \\ \frac{v_{eq}\omega^2}{\dot{M}} \end{bmatrix} M_u \tag{34}$$

$$v = \begin{bmatrix} 0 & 1 \end{bmatrix} \begin{bmatrix} \tilde{s} \\ \tilde{v} \end{bmatrix}. \tag{35}$$

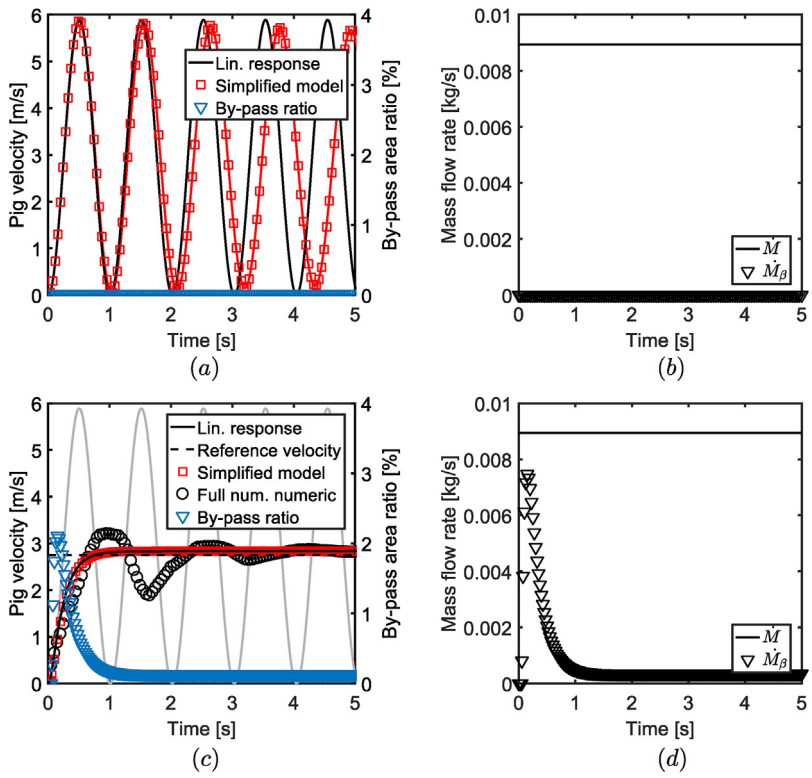

Fig. 13. (a) Pig velocity and by-pass opening without control. (b) Mass flow rate without control. (c) Pig velocity and by-pass opening with control. (d) Pig velocity and by-pass opening with control. (For interpretation of the references to colour in text, the reader is referred to the web version of the article.)

In the final step in obtaining Eq. (34) above we assumed for simplicity, without loss of generality, that $F_{fric,s} = F_{fric}$. The corresponding transfer function $P(\sigma)$ of the state space model reads:

$$P(\sigma) = \frac{\sigma \frac{v_{eq}\omega^2}{\dot{M}}}{\sigma^2 + \omega^2}. \tag{36}$$

Here σ denotes the complex frequency variable. A feedback loop with a linear controller $C(\sigma)$ may be constructed as shown in Fig. 12a.

The goal is to have no excursion in the pig velocity, and preferably it is equal or close to a preset reference velocity v_{ref}. Perhaps the simplest controller which would meet these requirements is a PD-controller:

$$C(\sigma) = K_p + K_d\sigma \tag{37}$$

The closed loop transfer function T as displayed in the equivalent blockdiagram in Fig. 12b then follows as:

$$T(\sigma) = \frac{\frac{v_{eq}\omega^2}{\dot{M}}}{\sigma^2 + \omega^2 + \frac{v_{eq}\omega^2}{\dot{M}}(K_p + K_d\sigma)} \tag{38}$$

We now again consider the example case which has been discussed in Section 4.2. For this case we have $\dot{M} = 0.0089$ kg/s and $F_{fric} = 40.80$ N. This yields a value of $v_{eq} = 2.94$ m/s and $\omega = 6.21$ rad/s, see Eqs. (9) and (14) respectively. The open loop response of the linear system to a mass influx $\dot{M}$ at $t = 0$ is marginally stable and is shown by the black line in Fig. 13a. Indeed when performing the numerical integration of Eq. (33) the pig velocity shows persisting oscillations, as shown by the red squares in Fig. 13a. We note that these numerical results for the 0% by-pass case are well captured by using the analytical approximation of Eq. (15), as shown by the red solid line. We now focus on damping the oscillation. The damping ratio of the second order system (Eq. (38)) can be identified as:

$$\zeta = \frac{\frac{v_{eq}\omega^2}{\dot{M}}K_d}{2\sqrt{\omega^2 + \frac{v_{eq}\omega^2}{\dot{M}}K_p}}. \tag{39}$$

Furthermore, we note that a constraint on the controller is that $\dot{M}_\beta$ has a maximum equal to $\dot{M}$.

The typical error in the velocity $\tilde{e}$ can be estimated as $-v_{eq}$, which is equal to the error in the beginning of a slip phase, as the actual pig velocity is still zero at that point. In a similar fashion, we estimate $\mathrm{d}\tilde{e}/\mathrm{d}t$ as $2v_{eq}\omega/\pi$, which is the average acceleration from 0 to $2v_{eq}$ in the time period π/ω. Using these estimations of $\tilde{e}$ and $\mathrm{d}\tilde{e}/\mathrm{d}t$ the following requirement can then be formulated:

$$K_p\tilde{e} + K_d\frac{\mathrm{d}\tilde{e}}{\mathrm{d}t} = -K_pv_{eq} + K_d\frac{2v_{eq}\omega}{\pi} = \dot{M}. \tag{40}$$

K_p and K_d can now be solved from Eqs. (39) and (40) and expressed as:

$$K_p = \frac{\dot{M}(16\zeta^2 - \pi^2)}{v_{eq}\pi^2}\ \mathrm{kg/m} \tag{41}$$

$$K_d = \frac{\dot{M}8\zeta^2}{v_{eq}\omega\pi}\ \mathrm{kg\,s/m}. \tag{42}$$

Oscillations will be damped when $\zeta > 1$. We choose a value of $\zeta = 1.2$, which yields $K_p = 0.0041$ kg/m and $K_d = 0.0018$ kg s/m. The result of this closed loop system is shown in Fig. 13c/d. The linear response of the closed loop system (black solid line), as well as numerical integration (red squares) indeed show that the pig velocity does not overshoot but now approaches the reference velocity (dashed black line), which has been set just below v_{eq} at a value equal to 2.75 m/s. In order to obtain this pig velocity trajectory, M_β and the corresponding by-pass opening have been increased for a short time

period to release the excess pressure of the upstream gas pocket. This is shown by the black triangles in Fig. 13d and the blue triangles in Fig. 13c respectively.

The simplified model relies on various assumptions, most notably the assumption that the pressure in the gas pocket upstream and downstream of the pig is instantaneously determined by the volume that the gas pocket occupies. The 1D full numerical model as described in Section 2.2, however, contains more physics and does not rely on this assumption. We now apply the controller derived from the simplified model directly on the full numerical model. The result is shown by the black circles in Fig. 13c. Although some oscillations are still present, the maximum pig velocity also in this case is clearly diminished. In very long pipelines the assumption of an instantaneous pressure response in the simplified model will not hold. It is therefore recommended for future research to further investigate the applicability of the simplified model in long pipelines. Instead of selecting the upstream mass M_u as a control parameter, a local pressure analysis around the pig may be more appropriate in this case.

The above example illustrates some minimum requirements on a controller which can be used to reduce pig velocity excursions in low pressure pipelines. In order to realize this in practice, the pig needs to be able to track at least the following quantities: pig velocity, pig acceleration, and the pressure upstream of the pig. Clearly the pig velocity needs to be measured in order to evaluate the error e compared to a preset desired reference velocity. The pig velocity is usually measured by odometer wheels attached to the pig which touch the inner pipe wall and thereby record the velocity, see for example [7]. The acceleration needs to be measured to evaluate $\mathrm{d}e/\mathrm{d}t$ to anticipate on a possible velocity excursion of the pig as soon as it starts moving. The acceleration can be measured with an accelerometer. Measurement of the upstream pressure will help to determine M_0, which is especially relevant when the local static friction $F_{fric,s}$ is larger than the dynamic friction F_{fric}.

5. Conclusions

The motion of by-pass pigs in a horizontal low pressure gas pipeline has been studied on a laboratory scale. The effect of the by-pass area and of the upstream bulk velocity was analyzed by means of an extensive experimental parameter study.

It was found that the average pig velocity can be well predicted by modeling the pressure loss through the by-pass with the Idelchik correlation and the friction between the pig and the pipe wall with a constant value. The use of the Idelchik correlation has been verified through previous CFD calculations, and is now confirmed experimentally. It was shown that under low pressure conditions the pig motion shows oscillatory motion with high pig velocity excursions due to gas accumulation that may build up behind the pig.

The frequency and amplitude of this oscillatory motion has been described with a simplified model which has been verified against experimental data. Based on the simplified model a PD controller has been formulated in order to reduce the pig velocity excursions. The controller was tested both in the simplified model as well as in a full numerical 1D transient model. In both cases it was shown that the pig velocity excursions are successfully mitigated by the controller. The case example which was used to test the controller thereby demonstrates minimum requirements for the design of a speed controlled pig in a low pressure pipeline.

For further research it is suggested to test a controller based on the simplified model in a laboratory environment while comparing the results with a 1D transient tool, as often these tools are used to predict the motion of a pig in a pipeline upfront. It is thus important that these 1D transient tools are able to capture the essential dynamics of a speed controlled pig in a low pressure pipeline. Based on these findings the controller can be further developed to take into account more physics, such as possible changes in friction while the pig is accelerating. In addition, the measurement of the pig velocity will in reality always contain a certain amount of noise. It is therefore recommended to investigate the sensitivity of the controller to a certain level of noise in a model environment first, before carrying out the experiment.

Acknowledgment

The work by the first author was funded by Shell Projects & Technology, for which they are greatly acknowledged.

Appendix A. Derivation of an analytic solution to the simplified model

When plugging in the equation for s_{eq} (Eq. (8)) into Eq. (11) we find:

$$\frac{p^*}{\rho^*}\frac{m}{(Ap_{out}+F_{fric})^2}\frac{\mathrm{d}^2\delta s}{\mathrm{d}t^2} = -\frac{\delta s}{M_0+\dot{M}t}. \tag{A.1}$$

When defining a_1 and a_2 as:

$$a_1 = \frac{p^*}{\rho^*}\frac{m}{(Ap_{out}+F_{fric})^2}M_0, \tag{A.2}$$

$$a_2 = \frac{p^*}{\rho^*}\frac{m}{(Ap_{out}+F_{fric})^2}\dot{M}, \tag{A.3}$$

we can cast Eq. (A.1) in a more general form:

$$\frac{\mathrm{d}^2\delta s}{\mathrm{d}t^2} = -\frac{\delta s}{a_1+a_2 t}. \tag{A.4}$$

A solution to Eq. (A.4) can be defined by using Bessel functions:

$$\delta s(t) = C_1 k \mathrm{J}_1(2k) - C_2 k \mathrm{Y}_1(2k), \tag{A.5}$$

with

$$k(t) = \sqrt{\frac{a_1+a_2 t}{a_2^2}}. \tag{A.6}$$

Here J_1 is the Bessel function of the first kind with order 1 and Y_1 is the Bessel function of the second kind with order 1. C_1 and C_2 are integration constants. A solution for $\delta v(t)$ can be obtained by differentiating Eq. (A.5):

$$\delta v(t) = \frac{1}{a_2}\left(C_1\mathrm{J}_0(2k) - C_2\mathrm{Y}_0(2k)\right). \tag{A.7}$$

Here J_0 is the Bessel function of the first kind with order 0 and Y_0 is the Bessel function of the second kind with order 0. We now substitute the values of a_1 and a_2 back into Eq. (A.6) and obtain equation:

$$\begin{aligned} k(t) &= \sqrt{\frac{a_1+a_2 t}{a_2^2}} = \sqrt{\frac{1}{a_1+a_2 t}}\left(\frac{a_1}{a_2}+t\right) \\ &= \sqrt{\frac{(Ap_{out}+F_{fric})^2}{\frac{p^*}{\rho^*}m(M_0+\dot{M}t)}}\left(\frac{M_0}{\dot{M}}+t\right). \end{aligned} \tag{A.8}$$

When using the definition for s_{eq}, Eq. (8), and subsequently the definition of the local angular frequency ω, Eq. (14), we can further simplify Eq. (A.8) and arrive at Eq. (13):

$$k(t) = \sqrt{\frac{(Ap_{out}+F_{fric})}{s_{eq}(t)m}}\left(\frac{M_0}{\dot{M}}+t\right) = \omega(t)\left(\frac{M_0}{\dot{M}}+t\right). \tag{A.9}$$

Similarly, we can rewrite Eq. (A.7) to obtain Eq. (15):

$$\begin{aligned}\delta v(t) &= \frac{1}{a_1 + a_2 t}\frac{a_1 + a_2 t}{a_2}\left(C_1 \mathrm{J}_0(2k) - C_2 \mathrm{Y}_0(2k)\right) \\ &= \omega^2(t)\left(\frac{M_0}{\dot{M}} + t\right)\left(C_1 \mathrm{J}_0(2k) - C_2 \mathrm{Y}_0(2k)\right).\end{aligned} \tag{A.10}$$

References

[1] J. Quarini, S. Shire, A review of fluid-driven pipeline pigs and their applications, J. Process Mech. Eng. 221 (1) (2007) 1–10.
[2] J. Cordell, H. Vanzant, The Pipeline Pigging Handbook, 3rd edition, Clarion Technical Publishers & Scientific Surveys Ltd., 2003, ISBN: 0-9717945-3-7.
[3] H.L. Wu, G. van Spronsen, Slug reduction with high by-pass pigs – a mature technology, 12th International Conference on Multiphase Production Technology, Barcelona (2005) 313–325.
[4] Q. Wang, C. Sarica, M. Volk, An experimental study on wax removal in pipes with oil flow, J. Energy Resour. Technol. Trans. ASME 130 (4) (2008) 0430011–0430015.
[5] C. Ramella, G. Canavese, S. Corbellini, M. Pirola, M. Cocuzza, L. Scaltrito, S. Ferrero, C.F. Pirri, G. Ghione, V. Rocca, A. Tasso, A.D. Lullo, A novel smart caliper foam pig for low-cost pipeline inspection – Part b: Field test and data processing, J. Pet. Sci. Eng. 133 (2015) 771–775.
[6] H.S. Lee, D. Agustiawan, K. Jati, M.A.H. Aulia, S.A. Thomas, S.P. Appleyard, By-pass pigging operation experience and flow assurance study, Offshore Technology Conference (2012) 1–10.
[7] N. Money, D. Cockfield, S. Mayo, G. Smith, Dynamic speed control in high velocity pipelines, Pipeline Gas J. 239 (8) (2012) 30–38.
[8] A. Singh, R.A.W.M. Henkes, CFD modelling of the flow around a by-pass pig, 8th North American Conference on Multiphase Technology (2012) 229–243.
[9] T. Nguyen, H. Yoo, Y. Rho, S. Kim, Speed control of pig using bypass flow in natural gas pipeline, in: 2001 IEEE International Symposium on Industrial Electronics Proceedings (ISIE 2001), vol. 2, Pusan, South Korea, 2001, pp. 863–868.
[10] M. Mirshamsi, M. Rafeeyan, Speed control of pipeline pig using the QFT method, Oil Gas Sci. Technol. 67 (4) (2012) 693–701.
[11] J. Tiratsoo, Pipeline Pigging Technology, 2nd edition, Gulf Professional Publishing, 1992, ISBN: 0-8720142-6-6.
[12] T.T. Nguyen, S.B. Kim, H.R. Yoo, Y.W. Rho, Modeling and simulation for pig with bypass flow control in natural gas pipeline, KSME Int. J. 15 (9) (2001) 1302–1310.
[13] M. Hendrix, H. IJsseldijk, W.-P. Breugem, R. Henkes, Development of speed controlled pigging for low pressure pipelines, 18th International Conference on Multiphase Production Technology, MPT 2017, June (2017) 501–509.
[14] H. IJsseldijk, By-Pass Pigging – Experiments and Simulations (Master's thesis), Delft University of Technology, 2016.
[15] I.E. Idelchik, Handbook of Hydraulic Resistance, 2nd edition, Hemisphere Publishing Corporation, 1987.
[16] M.H.W. Hendrix, X. Liang, W.-P. Breugem, R.A.W.M. Henkes, Characterization of the pressure loss coefficient using a building block approach with application to by-pass pigs, J. Pet. Sci. Eng. 150 (2017) 13–21.
[17] G.A. Groote, P.B.J. Van De Camp, P. Veenstra, G. Broze, R.A.W.M. Henkes, By-pass pigging without or with speed control for gas-condensate pipelines, Society of Petroleum Engineers – Abu Dhabi International Petroleum Exhibition and Conference, ADIPEC 2015 (2015).
[18] S.W. Churchill, Friction-factor equation spans all fluid-flow regimes, Chem. Eng. 84 (24) (1977) 91–92.
[19] J.E. Azpiroz, M.H.W. Hendrix, W.P. Breugem, R.A.W.M. Henkes, CFD modelling of bypass pigs with a deflector disk, 17th Int. Conf. on Multiphase Technology (2015) 141–155.
[20] B. Persson, Sliding Friction, Springer, 1998, ISBN: 3-540-63296-4.
[21] G. Tan, D. Wang, S. Liu, H. Wang, S. Zhang, Frictional behaviors of rough soft contact on wet and dry pipeline surfaces: with application to deepwater pipelaying, Sci. China Technol. Sci. 56 (2013) 3024–3032.
[22] K.H. Bendiksen, D. Malnes, R. Moe, S. Nuland, Dynamic two-fluid model OLGA. Theory and application, SPE Prod. Eng. 6 (2) (1991) 171–180.
[23] A. Goldszal, J.I. Monsen, T.J. Danielson, K.M. Bansal, Z.L. Yang, S.T. Johansen, G. Depay, LedaFlow 1D: simulation results with multiphase gas/condensate and oil/gas field data, 13th International Conference on Multiphase Production Technology (2007) 17–31.
[24] B. Sanderse, I.E. Smith, M.H.W. Hendrix, Analysis of time integration methods for the compressible two-fluid model for pipe flow simulations, Int. J. Multiphase Flow 95 (2017) 155–174.